Published online 10 April 2018 *Nucleic Acids Research, 2018, Vol. 46, No. 11* ***5487–5503***
doi: 10.1093/nar/gky260

Widespread enhancer activation via ERα mediates estrogen response in vivo during uterine development

Wendy N. Jefferson[1], H. Karimi Kinyamu[2], Tianyuan Wang[3], Adam X. Miranda[1], Elizabeth Padilla-Banks[1], Alisa A. Suen[1] and Carmen J. Williams[1,*]

[1]Reproductive & Developmental Biology Laboratory, National Institute of Environmental Health Sciences, NIH, Research Triangle Park, NC 27709, USA, [2]Epigenetics & Stem Cell Biology Laboratory, National Institute of Environmental Health Sciences, NIH, Research Triangle Park, NC 27709, USA and [3]Integrative Bioinformatics Support Group, National Institute of Environmental Health Sciences, NIH, Research Triangle Park, NC 27709, USA

Received January 22, 2018; Revised March 16, 2018; Editorial Decision March 26, 2018; Accepted March 27, 2018

ABSTRACT

Little is known regarding how steroid hormone exposures impact the epigenetic landscape in a living organism. Here, we took a global approach to understanding how exposure to the estrogenic chemical, diethylstilbestrol (DES), affects the neonatal mouse uterine epigenome. Integration of RNA- and ChIP-sequencing data demonstrated that ∼80% of DES-altered genes had higher H3K4me1/H3K27ac signal in close proximity. Active enhancers, of which ∼3% were super-enhancers, had a high density of estrogen receptor alpha (ERα) binding sites and were correlated with alterations in nearby gene expression. Conditional uterine deletion of ERα, but not the pioneer transcription factors FOXA2 or FOXO1, prevented the majority of DES-mediated changes in gene expression and H3K27ac signal at target enhancers. An ERα dependent super-enhancer was located at the Padi gene locus and a topological connection to the Padi1 TSS was documented using 3C-PCR. Chromosome looping at this site was independent of ERα and DES exposure, indicating that the interaction is established prior to ligand signaling. However, enrichment of H3K27ac and transcriptional activation at this locus was both DES and ERα-dependent. These data suggest that DES alters uterine development and consequently adult reproductive function by modifying the enhancer landscape at ERα binding sites near estrogen-regulated genes.

INTRODUCTION

In humans and mouse models, developmental exposure to estrogenic endocrine disruptors such as diethylstilbestrol (DES) causes morphological abnormalities of the reproductive tract, adult reproductive dysfunction and cancers of the reproductive system [for review, (1)]. However, in both human and mouse, short-term adult exposure to estrogenic chemicals has no long-term impact on the reproductive system. In a neonatal mouse model of exposure to DES (1 mg/kg/day), numerous gene expression differences occur during the time of exposure, but some of these persist into adulthood and correlate with functional changes, morphological effects, and uterine cancer (2–5). Why the developing reproductive tract is sensitive to estrogenic endocrine disruptors and the underlying mechanisms responsible for persistent gene expression changes are not known, but it is likely that changes in the epigenome are involved.

In support of this idea, DES exposure is associated with DNA methylation and gene specific changes in posttranslational modifications of histone tails that correspond to changes in gene expression later in life (2,5–9). These epigenetic changes may be explained in part by the finding that developmental exposure to DES significantly alters the levels of key histone modifying enzymes (5,10). In particular, the expression of HDAC1, 2 and 3 proteins in the uterus is severely reduced following neonatal DES treatment (5). Loss of HDAC activity could impair removal of acetyl groups from histone tails after the cessation of DES treatment and prolong signaling in the absence of estrogen.

There are no detailed studies examining how exposure to estrogenic compounds or other endocrine disruptors during development results in tissue specific changes in the epigenome on a global scale. Chromatin immunoprecipitation and whole genome sequencing to interrogate posttranslational modifications of histones that define distinct epigenetic states have been useful in determining epigenetic features in cultured cells treated with estrogenic compounds (11–14). Such studies provide an overview of epigenetic mechanisms underlying effects of estrogenic chemical exposure, but whether or not similar epigenome changes occur following developmental estrogen exposure is unknown. This information is essential for understanding how developmental exposures impact long term health outcomes.

*To whom correspondence should be addressed. Tel: +1 919 541 2158; Email: williamsc5@niehs.nih.gov

Here, we integrate genomic, epigenomic, and transcriptomic data to characterize the effects of DES exposure on chromatin state defined by type and localization of specific histone modifications and global gene expression. We find that genes differentially regulated by DES have significantly higher H3K27ac signal at both typical and super-enhancers previously identified as estrogen receptor α (ERα) binding sites. Indeed, in support of a role for ERα function in DES mediated changes in gene expression and enhancer landscape, we show that conditional deletion of ERα in the mouse uterus results in a loss of H3K27ac signal at the associated enhancers and prevents characteristic DES-induced changes in gene expression. This study demonstrates that estrogenic chemicals impact the epigenome of the developing reproductive tract and may result in reprogramming events that underlie permanent changes in gene expression, reproductive function, and adult-onset cancer.

MATERIALS AND METHODS

Resources table

Details of antibodies, chemicals, kits, deposited data, mouse lines, oligonucleotides, and software can be found in the Resources Table (Supplemental Table S1).

Animals

Animals were handled according to NIH/NIEHS guidelines under approved animal care and use protocols. Timed pregnant CD-1 mice were obtained from the in-house breeding colony at NIEHS (Research Triangle Park, NC, USA), housed in a temperature controlled environment (21–22°C) under a 12 h light:12 h dark cycle, and fed NIH-31 diet. At delivery, pups were randomly standardized to 10 female pups per dam. All female pups were treated by subcutaneous injections (0.02 ml) on the day of birth (postnatal day 1; PND1) through PND5 with either diethylstilbestrol (DES) 1 mg/kg/day dissolved in corn oil or with corn oil alone (controls) as described previously (5). Female pups were sacrificed on PND5, 4 h after the last injection. Uteri were collected, snap frozen on dry ice and stored at -80°C until further use.

Esr1$^{f/f}$ mice (C57BL/6NTac-Esr1<tm4.1>Ksk) were a gift from Kenneth Korach (NIEHS), Foxa2$^{f/f}$ (STOCK Foxa2<tm1Khk>) and Foxo1$^{f/f}$ mice (STOCK Foxo1<tm1Rdp>/J) were purchased from Jackson Labs, and PgR-cre mice (B6.129-Pgr<tm2(cre)Lyd>) were a gift from Francesco DeMayo (NIEHS). Conditional deletion of ERα, FOXA2 and FOXO1 in the uterus was accomplished by breeding floxed mice with Pgr-cre mice to generate Esr1$^{f/f}$;Pgr-cre+ (Esr1 cKO), Foxa2$^{f/f}$;Pgr-cre+ (Foxa2 cKO) or Foxo1$^{f/f}$;Pgr-cre+ (Foxo1 cKO). For all experiments, control females lacked the Pgr-cre transgene. Females from all three lines were treated neonatally with DES and uterine tissues were collected on PND5 as described for CD-1 mice above.

RNA isolation, real time RT-PCR, microarray analysis and RNA-seq

Total RNA was isolated from the uterus of individual control and DES-exposed mice on PND5 (n = 6/treatment group) using the RNeasy Kit and RNase-Free DNase Set (Qiagen, Valencia, CA) following the manufacturer's instructions. For real time RT-PCR, 1 ug total RNA determined by NanoDrop spectrophotemter with A_{260}/A_{280} > 1.9 was reverse transcribed using the First-Strand Synthesis System (Invitrogen, Carlsbad, CA, USA) following the manufacturer's instructions. Real time RT-PCR was performed using 25 ng of cDNA in a 25 ul reaction volume containing 12.5 uL of 2X Power SYBR green (Invitrogen) as described previously (5). A no RT control (Ct value not determined) was used as a negative control. Products were amplified using Applied Biosystems StepOnePlus Real-Time PCR System (Thermo Fisher) at 95°C for 10 min and then 40 cycles of 60°C for 1 min, 95°C for 15 s. Melting curves (60–95°C in 0.3°C increments) were performed on each primer set to confirm a single product and primer efficiency was confimed to be >75% for all primer sets. Primers were designed using Primer 3 (http://bioinfo.ut.ee/primer3) to span two exons to ensure RNA as the target and are listed in Supplemental Table S1. Ct values were determined by the StepOnePlus software (version 2.3) and all samples being compared were run at the same time. Expression levels were calculated using Microsoft Excel with the equation $2^{-(\text{Ct(gene)-Ct}(\textit{Ppia}))} \times 10\,000$; *Ppia* (cyclophilin A) was used as the house keeping gene for all experiments. There were no outliers in any of the data presented herein.

For microarray analysis, total RNA was isolated using the RNeasy Mini Kit and RNase free DNase set (Qiagen). Microarray was performed using Agilent Whole Mouse Genome 4 × 44 multiplex format oligo arrays (Agilent Technologies, Santa Clara, CA) as described previously (15). The CEL files were used to identify differentially expressed (DE) genes by the Genomics Suite Gene Expression workflow of Partek software package version 6.6 (Partek Inc., St. Louis, MO, USA). The Robust Multichip Analysis (RMA) algorithm with quantile for normalization and $\log_2$ transformation was applied to generate signal values of all samples. Differentially expressed genes were defined using the filters of ANOVA adjusted p value less than 0.05 and absolute fold change >2. All experiments were performed with at least triplicate with independent pools of RNA. Array data have been deposited in the Gene Expression Omnibus (GEO, accession GEO: GSE104402). Software EPIG (Extracting Patterns and Identifying co-expressed Genes) version 1.2 (16) was applied to extract patterns of co-expressed genes using the $\log_2$ transformed expression values generated from Agilent oligo arrays. The function of EPIG was used with perimeter setting 'Min cluster size = 3; Cluster resolution (correlation) = 0.6' for pattern extraction and 'SNR P-value = 0.05; r-value = 0.6' for gene categorization.

For RNA-seq, 1 μg of total RNA was sent to the NIH Intramural Sequencing Center to create a library using the TruSeq RNA kit (Illumina, San Diego, CA, USA) following the manufacturer's instructions and then sequenced. The RNA libraries were sequenced with a HiSeq 2000 system (Illumina). The raw RNA-Seq reads (101nt, paired-end) were initially processed by filtering with average quality scores >20. The reads passing the initial processing were aligned to the mouse reference genome (mm10; Genome Reference Consortium Mouse Build 38 from December 2011) using TopHat version 2.0.4 (17) and assembled using Cufflinks

version 2.0.2 (18). BigWig file was generated from normalized bedgraph file of each sample using bedGraphToBigWig. Scores represent normalized mapped read coverage. These bigWig files were displayed on UCSC genome browser as custom tracks. Expression values of RNA-Seq were expressed as FPKM (fragments per kilobase of exon per million fragments) values. Differential expression was calculated using Cuffdiff (18). Transcripts with FPKM >1, q-value < 0.05 and at least 1.5-fold differences were defined as differentially expressed (DE) genes. Hierarchical clustering and heatmap of DE genes were generated by the Genomics Suite of Partek software package version 6.6 (Partek Inc.).

Chromatin immunoprecipitation for analysis of histone modifications

For each biological replicate, whole uteri were pooled together (4–6 per sample) and pulverized on dry ice. The proteins were crosslinked with 1.0% formaldehyde in 1 ml PBS for 5 min at room temperature; the cross linking was quenched by addition of glycine (0.125 M final concentration). The fixative was removed and the samples were rinsed twice with cold PBS containing protease and phosphatase inhibitor cocktail (Sigma, St. Louis, MO, USA). Chromatin immunoprecipitation (ChIP) was performed as previously described (5) with the following modification. Immunocomplexes were captured using Protein A Dynabeads (Invitrogen) following the manufacturer's instructions. Antibodies to detect H3K4me3, H3K27me3, H3K27ac and H3K4me1 were from Active Motif.

Sequencing libraries were prepared from 100 ng precipitated DNA from each sample using the TruSeq RNA kit (Illumina). The DNA libraries generated for histone marks (H3K27me3, H3K4me3, H3K27ac, H3K4me1 and H3K27ac) were sequenced with a HiSeq 2000 system (Illumina). The raw ChIP-seq reads (51nt, paired-end) were processed by filtering with average quality scores >20. The reads were aligned to the mouse reference genome (mm10; Genome Reference Consortium Mouse Build 38 from December 2011) using Bowtie version 1.1.2 (19) with unique mapping and up to 2 mismatches for each read (-m 1 -v 2). The duplicated reads with the same sequence were discarded. The bigWig files were displayed on UCSC genome browser as custom tracks. Heatmaps of histone mark signal were generated by the Genomics Suite of Partek software package version 6.6 with 50 bp bin (Partek Inc.). The histone mark signal distribution around promoter regions (TSS ± 5 kb) was represented as the average reads per million uniquely mapped reads (RPM). Peak calling for each sample was performed by SICER version 1.1 (20) with FDR of 0.001. Differential peaks of histone marks between any pair of ChIP-seq samples were identified using MEDIPS software (21). Each differential region was defined as the genomic interval with at least 2-fold differences of read count and P-value ≤ 0.01. Each differential peak was mapped to nearby gene using software HOMER's 'annotatePeaks.pl' function (22). All the histone mark differential regions were assigned to genomic regions using web application PAVIS (23). The motif analysis of differential histone mark peak was performed using software HOMER's 'findMotifsGenome.pl' function with default setting (22). For super-enhancer analysis, differential H3K27ac peaks within 12.5 kb were merged. If the combined peak was larger than 15 kb, it was defined as a super-enhancer (24).

Histone purification and immunoblotting

For each biological replicate, histones were purified from two pooled uteri using the Histone Purification Mini Kit (Active Motif) following the manufacturer's instructions. For H3K27ac immunoblotting and gel staining, samples were desalted using Zeba™ Spin Desalting Columns (Thermo Fisher, Waltham, MA, USA). For gel staining, gel was rinsed with dH_2O, stained with Simply Blue (Thermo Fisher) for 1 h and rinsed with dH_2O. For H3K27ac immunoblotting, 2 μg of desalted purified histones was loaded onto a 12% SDS-PAGE gel (Bio-Rad, Hercules, CA, USA) and transferred to PVDF membrane. Immunoblotting was performed as previously described (5) with anti-H3K27ac (Active Motif) diluted 1:1000 in 5% milk in TBS-T as the primary and donkey anti-rabbit (Jackson Immunolabs) diluted 1:25 000 in 1% milk in TBS-T. Bands were visualized with Super Signal West Femto (Themo Fisher) and imaged using Chemi Doc Touch Imaging System (Bio-Rad).

For FOXA1 and actin immunoblotting, nuclear proteins were extracted from single uteri using NE-PER kit following the manufacturer's instructions (Thermo Fisher). 10 ug of nuclear protein was loaded onto 10% SDS-PAGE gels (Bio-Rad) and transferred to PDVF membrane (Bio-Rad). HeLa cell nuclear extract (1 ug; Active Motif) was loaded as a positive control. Immunoblotting was perfomed as previously described (5) with anti-FOXA1 (Abcam) diluted 1:1000 and anti-actin (Sigma) diluted 1:1000 in 5% milk in TBS-T as the primary antibodies; donkey anti-rabbit (Jackson ImmunoResearch) and goat anti-mouse (Jackson ImmunoResearch) diluted 1:25 000 in 1% milk in TBS-T as the secondaries, respectively. Bands were visualized with Super Signal West Femto (Themo Fisher) and imaged using the Chemi Doc Touch Imaging System (Bio-Rad).

For modified citrulline immunoblots, total proteins were extracted from single uteri using T-PER (Thermo Fisher). 20 μg of total proteins were loaded onto 4–20% SDS-PAGE gels (Bio-Rad) and transferred to PVDF membrane (Bio-Rad). Citrulline was modified and detected on the blots using the anti-citrulline (modified) detection kit (Millipore, Burlington, MA) following the manufacturer's instructions. Images were captured using Chemi Doc Touch Imaging System (Bio-Rad).

Chromatin conformation capture assay (3C PCR)

For each biological replicate, uteri were pooled (4–5 uteri per sample). Proteins were crosslinked to chromatin with 1.0% formaldehyde in PBS for 10 min at room termperature; crosslinking was quenched in 0.125 M glycine. Samples were centrifuged for 8 min at 225 × g at 4°C and fixative was removed. Pellets were resuspended in 5 ml of immunoprecipitation buffer (50 mM Tris-HCl, pH 7, 1% Nonidet P-40) then centrifuged for 5 min at 400 × g at 4°C. The supernatant was removed and restriction digestion, ligation, and DNA purification was carried out according to the protocol in (25). 3C DNA from PND5 Co and DES was amplified

using ReadyMix™ REDTaq® PCR Reaction Mix (Sigma) and the *Padi1* 3C HindIII primers (Supplemental Table S1). PCR products were separated on 1% agarose gels and the bands of the expected product size of 244 bp were excised. DNA was isolated from the gel fragments using QIAquick Gel Extraction Kit (Qiagen) and sequenced commercially (Genewiz, South Plainfield, NJ). 3C DNA from PND5 Co Esr1 WT, Co Esr1 cKO, DES WT, and DES Esr1 cKO was amplified by real time PCR using SYBR green as described for real time RT-PCR. Products were run on 2% agarose gels to confirm a single band of the correct size.

Data deposition

The raw and processed RNA-seq, microarray, and ChIP-seq datasets reported in this study have been submitted to the NCBI Gene Expression Omnibus (www.ncbi.nlm.nih.gov/geo) with accession number GSE104402.

RESULTS

Neonatal DES exposure increases H3K27ac association across the genome in the mouse uterus on postnatal day 5 (PND5)

To elucidate the epigenetic state of normally developing tissue, we performed chromatin immunoprecipitation coupled with high-throughput sequencing (ChIP-seq) of histone modifications typically associated with active (H3K4me3, H3K27ac) or repressed (H3K27me3) transcription in PND5 uteri from control (Co) and DES-exposed mice. Genome-wide peak calling analysis by SICER (20) indicated similar numbers of H3K27me3 (4848 in Co versus 5587 in DES) or H3K4me3 (12 650 in Co versus 13 817 in DES) peaks, respectively. However, there was a striking 42% increase in the number of H3K27ac peaks within DES-exposed uteri (18 866 in Co versus 26 848 in DES). Analysis of the peak overlap between the two treatment conditions revealed that only about half of the H3K27me3 peaks (∼44%) identified in the DES-exposed group were also found in controls, whereas almost all H3K4me3 peaks (∼88%) were common to both groups (Figure 1A). In contrast to H3K27me3 and H3K4me3, there was a prominent increase in the total number of H3K27ac peaks that were unique to uteri from DES-exposed mice relative to the peaks unique to controls (∼2.4-fold). These findings indicate that there were significant differences in genomic space enriched with H3K27me3 and H3K27ac signal following DES treatment, whereas H3K4me3 enriched chromatin was within similar genomic loci in the two treatment groups. To determine if the gain in H3K27ac was at the same locations as a loss in H3K27me3, we performed a differential coverage analysis with MEDIPS (21) and overlapped the resulting data sets. This analysis is more sensitive than SICER and generates a higher number of smaller peaks. Only 174 peaks overlapped between H3K27me3 peaks (10 810) that were lost and the H3K27ac peaks (37 144) that were gained, indicating that the vast majority of the H3K27ac sites were new and distinct from sites marked with H3K27me3. Next, we asked whether DES induced an overall change in the genomic distribution of the three histone marks. In general, the genomic distribution of the three histone marks did not differ between Co and DES-exposed uteri (Figure 1B).

We next examined whether there were global differences in the binding patterns of the three histone marks at the transcription start sites (TSS). We performed a composite analysis of the ChIP signal of all the annotated TSS ± 5 kb relative to the TSS. Annotated TSS of DES-exposed uteri had significantly higher H3K27ac signal compared to control uteri, whereas H3K27me3 and H3K4me3 signal at all TSS were similar between the two groups (Figure 1C). These findings suggest that alterations in H3K27ac could mediate gene expression differences in response to DES treatment.

ChIP-seq signal of H3K27ac at the TSS correlates with DES-mediated gene expression changes

To determine whether differential association of histone H3 marks at the annotated TSS upon DES treatment was associated with gene expression changes, we performed RNA-seq on uteri collected from PND5 Co and DES-exposed mice 4 h after the last injection. Consistent with previous reports (26), 4498 genes were significantly altered in DES-exposed mice, with 2345 up- and 2153 down-regulated, respectively (Figure 2A).

We next examined whether the density of the ChIP signal at the TSS for each of the three histone marks had an impact on the expression of 4498 genes altered by DES treatment. Genes altered by DES did not show a significant change in H3K27me3 ChIP signal compared to control (Figure 2A; left panel). Analysis of the H3K4me3 signal revealed a subtle increase in association of this mark at the TSS of DES-induced up-regulated genes, which can also be observed in the differential ChIP signal (Figure 2A, middle panel). Notably, H3K27ac association at the TSS was markedly higher at genes up-regulated by DES compared to control (Figure 2A, right panel). Interestingly, we also noted a subtle increase in association of this mark at the TSS of some genes that were down-regulated by DES treatment. These data indicate that increased association of this mark at the TSS correlates with a chromatin state that translates not only into a robust activation of genes (up-regulation) but also active repression of a subset of DES target genes (down-regulation).

Examples of the most predominant patterns of these three marks at the TSS for both up- and down-regulated genes are shown (Figure 2B). As expected, there was increased H3K4me3 and decreased H3K27me3 at the TSS of both *Oxtr* and *Six1* (up-regulated genes), but only *Oxtr* had increased H3K27ac. There was also a broad region of H3K27me3 association at the *Six1* locus, suggesting general repression of this homeobox transcription factor in this tissue (5). However, there was a small decrease in H3K27me3 association centered at the TSS in the DES group that aligns with characteristic up-regulation of expression following DES treatment. The down-regulated gene, *Wnt6*, showed the anticipated decrease in H3K4me3 and H3K27ac but no significant difference in H3K27me3 at the TSS.

To further determine whether this difference in H3K27ac at the TSS was solely due to changes in gene expression, we divided the data into two categories, unchanged and differentially altered genes. Analysis of normalized H3K27ac

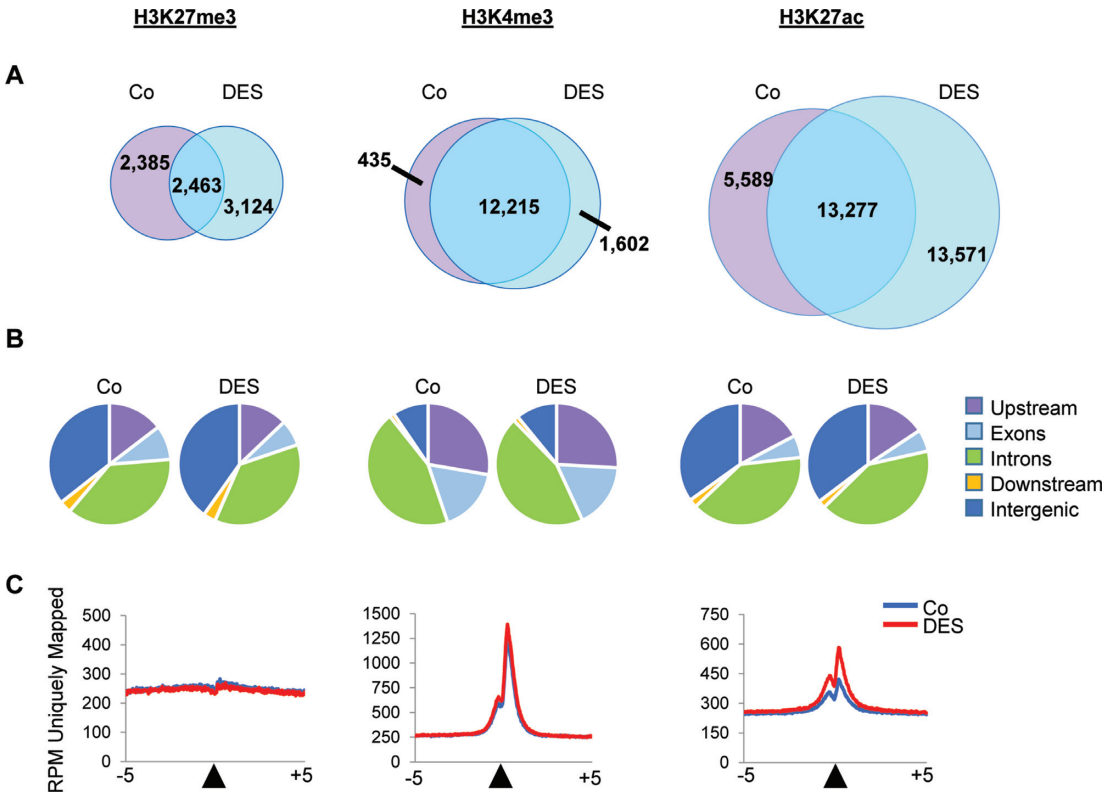

Figure 1. Genomic distribution of histone H3K27me3, H3K4me3 and H3K27ac following neonatal DES treatment.) (**A**) Venn diagrams showing overlapping peaks between Co and DES-exposed samples for each histone mark. (**B**) Pie charts illustrating percentage genomic distribution of each histone mark in Co and DES-exposed uterine samples. The legend on the right indicates the genomic features. (**C**) Metaplots depicting the enrichment patterns (reads per million uniquely mapped) of the histone marks for all TSS ± 5 kb of annotated genes. Closed triangle indicates TSS.

signal around the TSS revealed that global H3K27ac signal was higher at the TSS of DES-exposed samples compared to controls independent of changes in gene expression (Figure 2C). However, the level of H3K27ac signal at the TSS of genes differentially altered by DES was generally higher than at the TSS of unchanged genes (Figure 2C). These data further indicate that neonatal uteri exposed to DES exhibit a global increase in H3K27ac signal across the genome. Importantly, the increase in H3K27ac association with the genome was not associated with a global increase in the amount of H3K27ac protein in DES-exposed uteri (Figure 2D).

DES remodels enhancer-like features of differentially expressed genes

Given that there was a global increase in H3K27ac signal at the annotated TSS of DES-exposed uteri (Figures 1C and 2C) and that the majority of the H3K27ac associated regions were outside the promoter/TSS region (Figure 1B), we examined whether the intensity of the H3K27ac signal at regions distal to TSS (±100 kb but not within ±5 kb of TSS) was different at the 4498 genes altered by DES treatment. Differential analysis of the H3K27ac signal within these regions (>1.5-fold change in signal intensity, DES versus Co), yielded 12 222 peaks. H3K27ac enrichment at genomic regions distal to TSS is generally associated with enhancers, suggesting that the differential H3K27ac peaks were within putative enhancer regions. Of note, the differential enhancer regions were also associated with 70% of genes altered by DES treatment.

These data suggested that DES induced gene expression changes were predominantly driven by increased H3K27ac signal at putative enhancers and TSS (Figures 1B, 2C). Indeed, assigning the differential H3K27ac enhancer signal based on the intensity associated with the nearest differentially expressed gene revealed a larger impact on enhancers associated with up-regulated genes (7630 peaks associated with 1685 genes) as opposed to down-regulated genes (4592 peaks associated with 1327 genes) (Figure 3A). Two patterns emerged from this analysis. The major pattern indicated that the increase and decrease in H3K27ac occupancy was correlated with an increase or decrease in gene expression, respectively (Figure 3A, green boxes). The minor pattern represented up-regulated genes that lost H3K27ac signal and down-regulated genes that gained H3K27ac signal (Figure 3A, red boxes), suggesting active repression of these enhancers upon DES treatment. In addition to the two patterns of H3K27ac occupancy, further analysis revealed that 67% of the genes differentially regulated by DES had enriched H3K27ac signal at presumed enhancers and the corresponding TSS, a characteristic generally associated with cis-regulatory DNA elements that control gene activation (27).

To verify that the differentially H3K27ac enriched regions were active enhancers, we performed ChIP-seq anal-

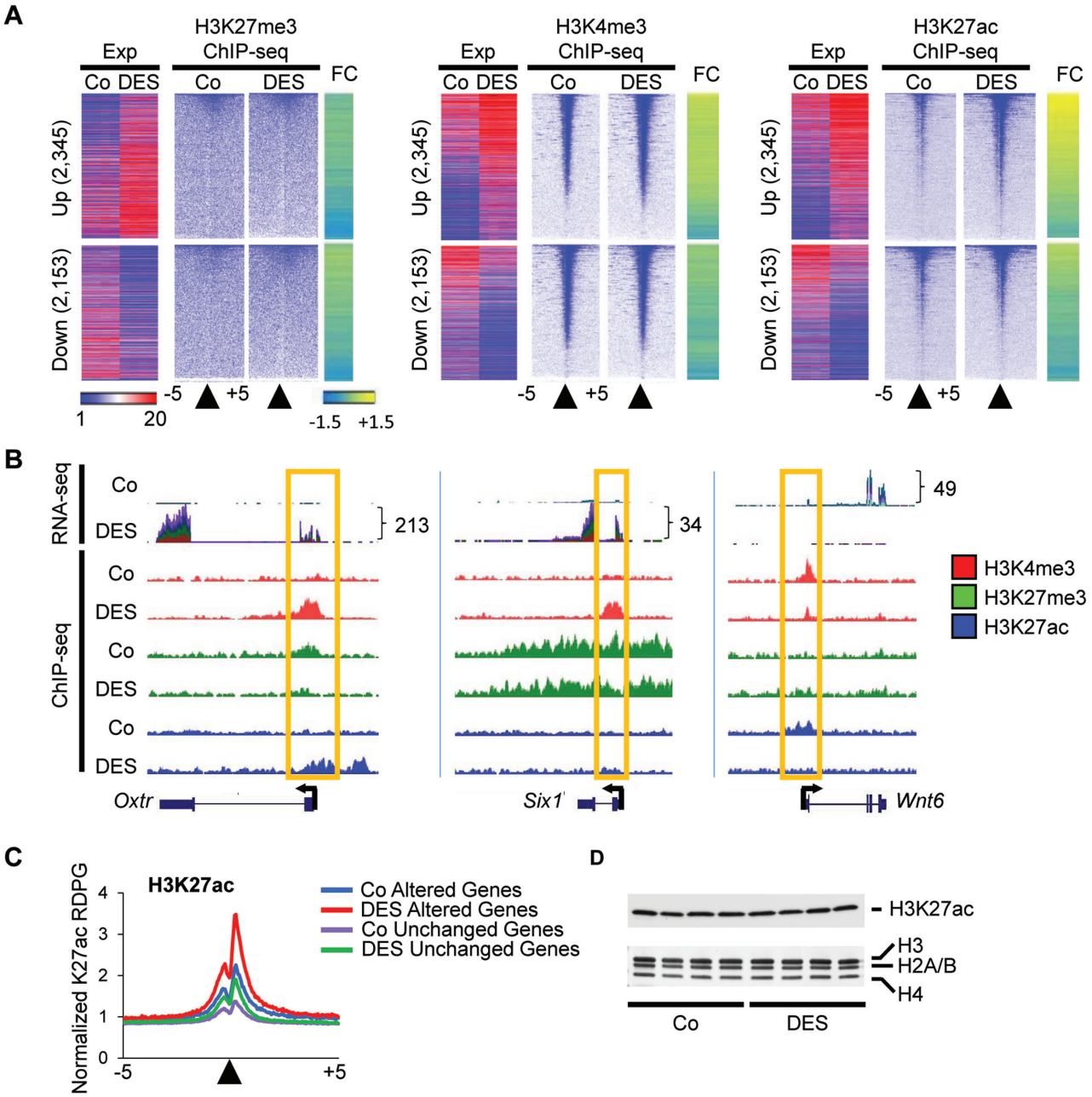

Figure 2. H3K27ac is enriched at TSS of differentially expressed genes following neonatal DES treatment. (**A**) Heatmaps displaying H3K27me3, H3K4me3 and H3K27ac ChIP-seq signal mapping to a 5 kb window around TSS of 4498 differentially expressed genes, up- and down-regulated (top and bottom panel), respectively. Closed triangle indicates TSS. Left panel: Heat maps depicting normalized expression (FPKM) for both the up- and down-regulated genes ranked by the highest to lowest ChIP signal of the respective histone mark in DES-exposed sample. Right panel: Differential change in ChIP signal DES versus Co [fold change (FC)] of each histone mark. (**B**) Representative UCSC browser shots showing ChIP profiles of H3K27me3 (green), H3K4me3 (red), H3K27ac (blue); differentially expressed genes are indicated by the RNA-seq track. Arrows denote the direction of transcription and gold boxes demarcate the TSS region. (**C**) Metaplots depicting the enrichment patterns (reads per million uniquely mapped) of H3K27ac at TSS ± 5 kb of differentially expressed genes. Closed triangle indicates TSS. (**D**) Immunoblot showing H3K27ac expression (top panel). Duplicate gel of same histone samples stained with Simply Blue (bottom panel) as a loading control; histone H3, H2A/B and H4 indicated. Samples were from total histones isolated from Co and DES-exposed uteri ($n = 4$ uteri/group).

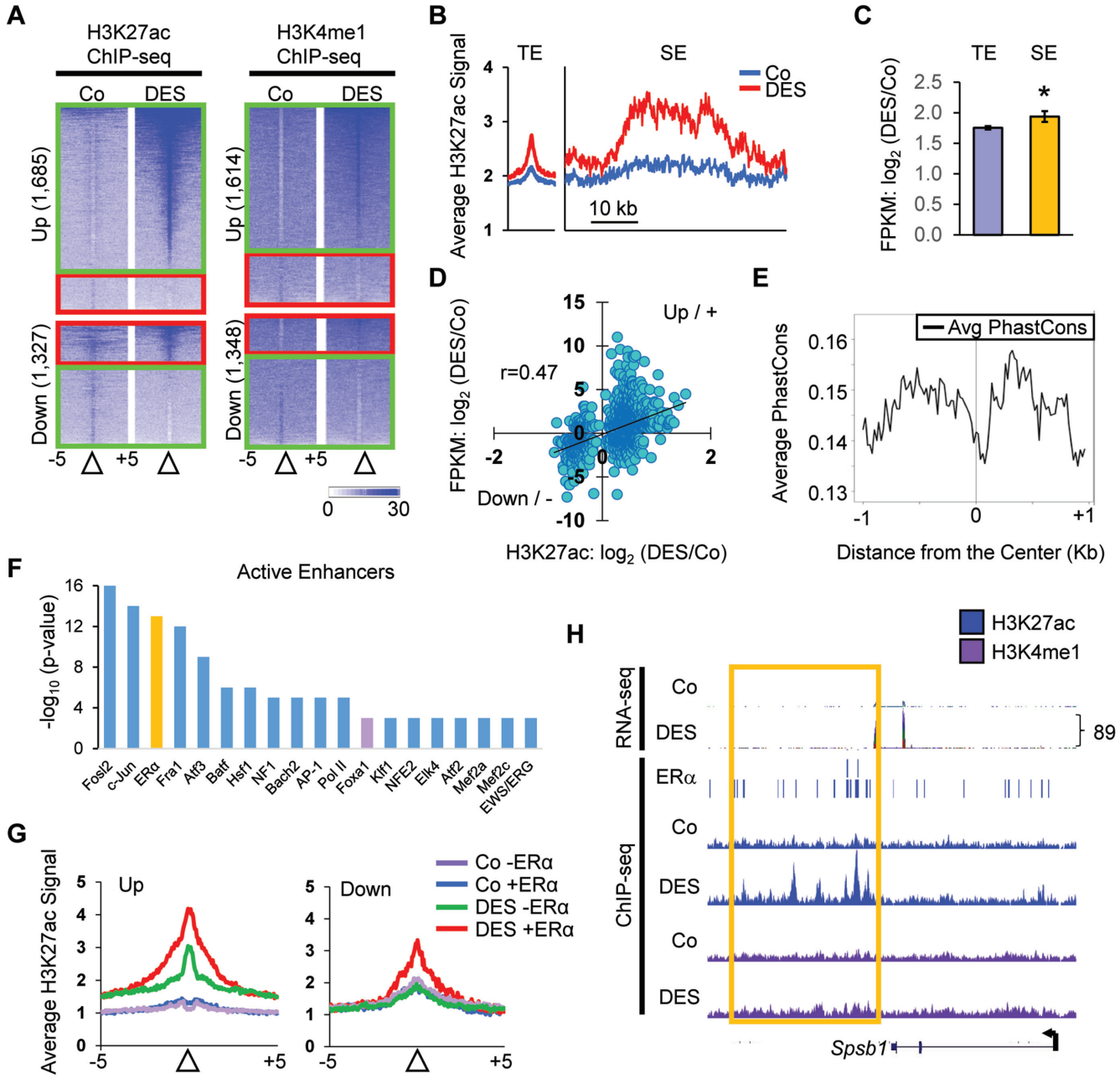

Figure 3. DES treatment induces active and super-enhancers at ERα binding sites to modulate gene expression. (**A**) Heat maps displaying H3K27ac and H3K4me1 ChIP signal enriched at differential peaks ± 100 kb (excluding TSS) of altered genes. ChIP signal from up- or down-regulated genes in Co and DES-exposed samples is sorted by highest to lowest signal in DES-exposed samples. Green boxes highlight positively correlated differential ChIP signal and gene expression, whereas red boxes denote an inverse correlation. The number of altered genes in each category is shown on the left. ChIP signal is plotted against the center of the peak ± 5 kb. Open triangle indicates center of peak. (**B**) Metaplots of average H3K27ac ChIP signal at typical enhancers (TE; $N = 6249$) and super-enhancers (SE; $N = 380$). Graphs use same axis scales; scale bar = 10 kb. (**C**) Bar graph showing gene expression (FPKM of $\log_2$ DES/Co) associated with TE or SE; $P < 0.05$. (**D**) Correlation between gene expression changes (FPKM of $\log_2$ DES/Co) and density of H3K27ac signal (RPM $\log_2$ DES/Co) at active enhancers. For each gene, data plotted is the largest fold change in H3K27ac density (DES versus Co). Gene expression is positively correlated $r = 0.47$ with H3K27ac density at active enhancers. (**E**) Average PhastCons score at the enhancers' center-of-the-peak ± 1 kb is plotted. (**F**) Known motifs enriched at DES-mediated active ehancers with an enrichment P-value <0.01 are plotted ($-\log_{10}$, P-value). (**G**) Metaplots of H3K27ac signal at enhancers associated with up-regulated (left) and down-regulated (right) genes. Open triangle indicates center of peak. H3K27ac peak density is sorted based on presence or absence of ERα binding site in Co or DES sample (43). (**H**) Genome browser view of RNA-seq paired with ChIP-seq signal for H3K27ac (blue) and H3K4me1 (purple) and ChIP-seq tracks for ERα binding sites (43) from ovariectomized adult mice (top track, vehicle; bottom track, E2-1hr) at *Spsb1* locus. Gold box highlights a region with a high density of ERα binding sites and differential H3K27ac/H3K4me1 enrichment.

ysis of H3K4me1 because genomic regions enriched with both H3K4me1 and H3K27ac generally represent active enhancers (28–31). H3K4me1 enrichment at genes up- or down-regulated by DES treatment was similar to that observed for H3K27ac, confirming that the two histone marks largely associate with active enhancers and predominantly enhance gene activation (Figure 3A). Together, these findings suggest that differential association of H3K27ac and H3K4me1 at enhancer regions is a major mechanism by which DES exerts its impact on gene expression *in vivo*.

DES mediates the formation of super-enhancers near altered genes

Our analysis above indicated that differential H3K27ac signal was the predominant determinant of DES driven changes in gene expression. In addition, we observed that some of the H3K27ac peaks appeared to cover large genomic regions (larger than the 10 kb), a characteristic of genomic space recently termed as super-enhancers (24). Super-enhancers are large genomic regions that are largely depleted of nucleosomes to accommodate high transcription factor binding capacity, ultimately to control the expression of important genes in development and disease (24,32–34). Based on the above observation, we analyzed the 12 222 differentially associated H3K27ac enhancer peaks that were ±100 kb of the TSS of altered genes for the presence of super-enhancers. For this analysis, we stitched together enhancers that were <12.5 kb apart, grouped them into either typical enhancers (TE) defined as stitched peak width <15 kb or super-enhancers (SE) defined as stitched peak width >15 kb, and then displayed the average H3K27ac signal for both Co and DES-exposed samples (Figure 3B). The analysis revealed 6249 typical enhancers and 380 super-enhancers, respectively. Consistent with other features that define super-enhancers, analysis of MED1 ChIP-seq peaks from mouse ES cells (24) revealed that ∼34% (128/380) of the super-enhancers also had MED1 peaks. In contrast, MED1 peaks were found only in ∼4% of the typical enhancers. In addition to the large size of the region, the peaks at super-enhancers had higher levels of H3K27ac signal over the entire region compared to typical enhancers. Small but significantly higher fold increases in gene expression (mean ∼14%) were seen in genes associated with super-enhancers versus typical enhancers (Figure 3C). Moreover, most super-enhancers were associated with up-regulated genes (75%) suggesting that H3K27ac-enriched super-enhancers are a major mechanism by which DES causes increases in gene expression in the developing mouse uterus.

DES associated active enhancers are correlated with gene expression and are moderately conserved

To further understand the mechanism underlying gene regulation during DES treatment, we identified active enhancers by selecting the differential H3K27ac enhancer peaks that overlapped H3K4me1 peaks within the same gene regions and then ranked them according to their associated gene expression (27). This analysis identified 4325 active H3K27ac enhancer peaks that were associated with 1415 altered genes. H3K27ac occupancy at the active enhancers was directly correlated with gene expression ($r = 0.47$) (Figure 3D). Because developmental exposures to DES have been linked to poor reproductive health outcomes in humans (1), we next examined whether DNA elements within the DES driven H3K27ac active enhancers in the mouse uteri were conserved within mammalian species. Enhancer peak regions (center of peak ± 1 kb) were analyzed for sequence conservation using PhastCons (35). A PhastCons score of 0.1 to 0.5 indicates moderate to high conservation, respectively (36). The H3K27ac enriched active enhancers in mouse uteri had an average PhastCons score ranging from 0.14 to 0.155 suggesting a moderate level of conservation and potential importance in gene regulation across mammalian species (Figure 3E).

DES-dependent active enhancers are highly enriched in ERα motifs

Active enhancers are comprised of gene regulatory elements that are largely depleted of nucleosomes, making them 'hotspots' of transcription factor binding (11).To identify potential mediators of DES-driven changes in gene expression, we determined the enrichment of transcription factor motifs within the differential active enhancer elements using HOMER (22). Nineteen transcription factor motifs were significantly enriched within the enhancer elements; $P < 0.01$ (Figure 3F). Consistent with the finding that DES acts through ERα (37), one of the most hightly enriched motifs was the ERα binding site. In addition, characteristic binding motifs typically enriched in other models of estrogen signaling were also enriched including Foxa, Bach, Fos, Jun, Atf, AP-1, Klf and Pol II (12,38–41). Enrichment in Fos and Jun-related motifs is consistent with previous reports indicating that ERα can act through a DNA-binding-independent interaction with AP-1 and SP1 transcription factors [reviewed in (40)]. It is also consistent with a recent paper describing direct interactions between ERα and JUN as well as ChIP-seq data demonstrating extensive overlap between ERα and JUN DNA binding sites (41). In contrast to the motif analysis of active enhancers, motif analysis of TSS regions that had differential H3K27ac revealed far less significant enrichment of ERα motifs at up-regulated genes, and no enrichment at down-regulated genes (Supplemental Table S2). The lack of ERα at the TSS of down-regulated genes suggests that gene repression is mediated by ERα-enhancer interactions, not those at TSS.

In the active enhancer analysis, Fosl2 and c-Jun were the two most highly enriched motifs, and both are associated with estrogen-repressed genes in MCF-7 cells (42). To determine if this association was also observed in the uterus, we performed additional motif analysis. For this analysis, we separated the enhancers based on their association with either the up- or down-regulated genes, and then performed a separate analysis of the motifs associated with the subset of active enhancers with increased H3K27ac near down-regulated genes (Supplemental Table S2). This new analysis identified ERα, Fosl2, and c-Jun as the most highly significant motifs associated with up-regulated genes. Pioneer transcription factor motifs including BATF, GATA, and FOXA1 were also enriched in these enhancers. When

all down-regulated genes were considered, ERα motifs were not significantly enriched; however, there was enrichment of ERα motifs in the subset of enhancers with increased H3K27ac associated with down-regulated genes. In addition, FOXA2 and GATA motifs were enriched near this subset of down-regulated genes, suggesting that pioneer factors may also have a role in ERα-mediated gene repression.

Because ERα-binding motifs were highly enriched in the active enhancer regions, we compared the 4325 differential active enhancer regions in this dataset with a previously published ERα ChIP-seq data set that identified ERα-binding sites in chromatin from adult mouse uterine tissue (43). For this analysis, we combined all the genomic regions in the published dataset that had ERα binding sites [vehicle and estradiol (E2) treatment for 1 h data sets were combined]. Of note, the published data set from Hewitt *et al.* (2012), was derived from adult uteri of ovariectomized C57BL/6 mice that had been treated with either vehicle or E2 for 1 h. In contrast, the differential enhancers in our dataset were identified in uteri from CD-1 neonatal mice treated with vehicle or DES for 5 days before collection. Despite differences in the model systems and treatment conditions, there was significant overlap between the ERα binding sites and differential H3K27ac enriched peaks from DES-exposed uteri. Of the 3080 H3K27ac enriched peaks associated with up-regulated genes, 1270 (41%) overlapped with an ERα ChIP-seq peak and of the 1245 peaks associated with down-regulated genes, 345 (28%) overlapped with an ERα binding site (Supplemental Figure S1A). Interestingly, for the up-regulated genes, regions containing ERα binding sites appeared to have more H3K27ac signal compared to the regions lacking ERα binding sites. Analysis of the average H3K27ac signal in up- and down-regulated genes based on the treatment condition and the presence of an ERα binding site revealed a clear increase in H3K27ac signal in peaks that were associated with and ERα binding sites relative to those that were not (Figure 3G and Supplemental Figure S1B). This finding was most prominent in up-regulated genes but this excessive increase in signal associated with ERα binding sites was also observed in the down-regulated genes (Figure 3G and Supplemental Figure S1B). Mechanistically, this finding suggests that DES-mediated increase and decrease in gene expression is associated with large increases in H3K27ac at active enhancers that are enriched for ERα binding.

The *Spsb1* locus is an example of a region that exhibited H3K27ac enriched differential enhancer peaks overlapping ERα-binding sites associated with increased *Spsb1* gene expression observed in RNA-seq (Figure 3H). Of note, this region also met the criteria for a super-enhancer region. Additional examples representing up-regulated (*Nxnl2*) and down-regulated genes (*Hand2* and *Col26a1*) showing the gene expression pattern and associated combinations of increased or decreased H3K27ac and H3K4me1 are shown (Supplemental Figure S1C–E).

ERα, but not FOXA2 or FOXO1, is required for DES-mediated gene expression

To definitively determine if there was a requisite role for ERα in DES mediated changes in chromatin state and gene expression, we generated a conditional knockout of ERα in the mouse uterus using the Pgr-cre transgene ($Esr1^{f/f}$;Pgr-cre), referred to as 'Esr1 cKO' mice. $Esr1^{f/f}$ littermates, referred to as 'WT', served as controls. Microarray analysis was performed to identify genes differentially expressed between Co and DES-exposed WT and Esr1 cKO mice, henceforth referred to as Co-WT, DES-WT, CO-Esr1 cKO and DES-Esr1 cKO. Of note, the background strain of these mice is C57BL/6, whereas CD-1 mice were used in generating all data in Figures 1–3. We performed gene expression pattern analysis [EPIG (16)] to compare intensity values of all probes on the microarray and to identify the probes with similar expression patterns among the three groups of interest for determining how the absence of ERα impacted the DES response: Co-WT, DES-WT, and DES-Esr1 cKO (Figure 4A). Two major gene expression patterns accounted for most of the altered gene expression: genes up-regulated by DES in the WT and protected from DES in Esr1 cKO (pattern 1), and genes down-regulated by DES in the WT and protected from DES in the Esr1 cKO (pattern 6). We next filtered the genes represented in the two patterns into those that were significantly changed between Co-WT and DES-WT ($P<0.05$) with a cutoff of >2-fold difference and average signal intensity of >100 in at least one treatment group (up-regulated, 2389; down-regulated, 2228). The majority of significantly altered genes were contained within one of these two gene expression patterns (~90%; Figure 4B, Venn diagrams) and were protected by ERα deletion (Figure 4B; heat maps). These findings confirm that DES-induced gene expression changes in the neonatal uterus are ERα dependent. This list of 4,130 protected genes will be used in our later analysis of the dependence of specific histone modifications on the presence of ERα.

FOXA1 is required for ERα-mediated enhancer activation in human cell lines (11,12,44,45). In addition to ERα binding site motif enrichment at the H3K27ac peaks, FOX-binding site motifs also were enriched at active enhancers (Figure 3D). Furthermore, several Fox genes were highly up-regulated by DES exposure (Supplemental Figure S2A); *Foxa1* was not expressed above the gene expression filtering cutoffs described above in any samples examined in this study (microarray and RNA-seq; data not shown). In addition, FOXA1 protein was not detected by immunoblot (Supplemental Figure S2B). Foxo1 and Foxa2 were chosen for further investigation because expression of these two genes was very low or absent in controls and highly up-regulated after DES. To determine whether FOXA2 or FOXO1 contributed to DES-induced uterine gene expression changes, we used the Pgr-cre transgene to generate both Foxa2 uterine conditional knockout (Foxa2 cKO) and Foxo1 uterine conditional knockout (Foxo1 cKO) mice that were then either Co or DES-exposed. Microarray analysis was performed on PND5 uteri from DES-exposed $Foxa2^{f/f}$ (WT), Foxa2 cKO, $Foxo1^{f/f}$ (WT) and Foxo1 cKO mice. Analysis of gene expression changes in DES-exposed $Foxa2^{f/f}$ and Foxa2 cKO samples resulted in only 295 genes that were significantly changed ($P < 0.05$) using a cutoff of >2-fold difference and average intensity of >100 in at least one group. Even fewer (108) significantly different genes were identified when comparing DES-exposed $Foxo1^{f/f}$ versus Foxo1 cKO. Alterations in these ~400 genes from both

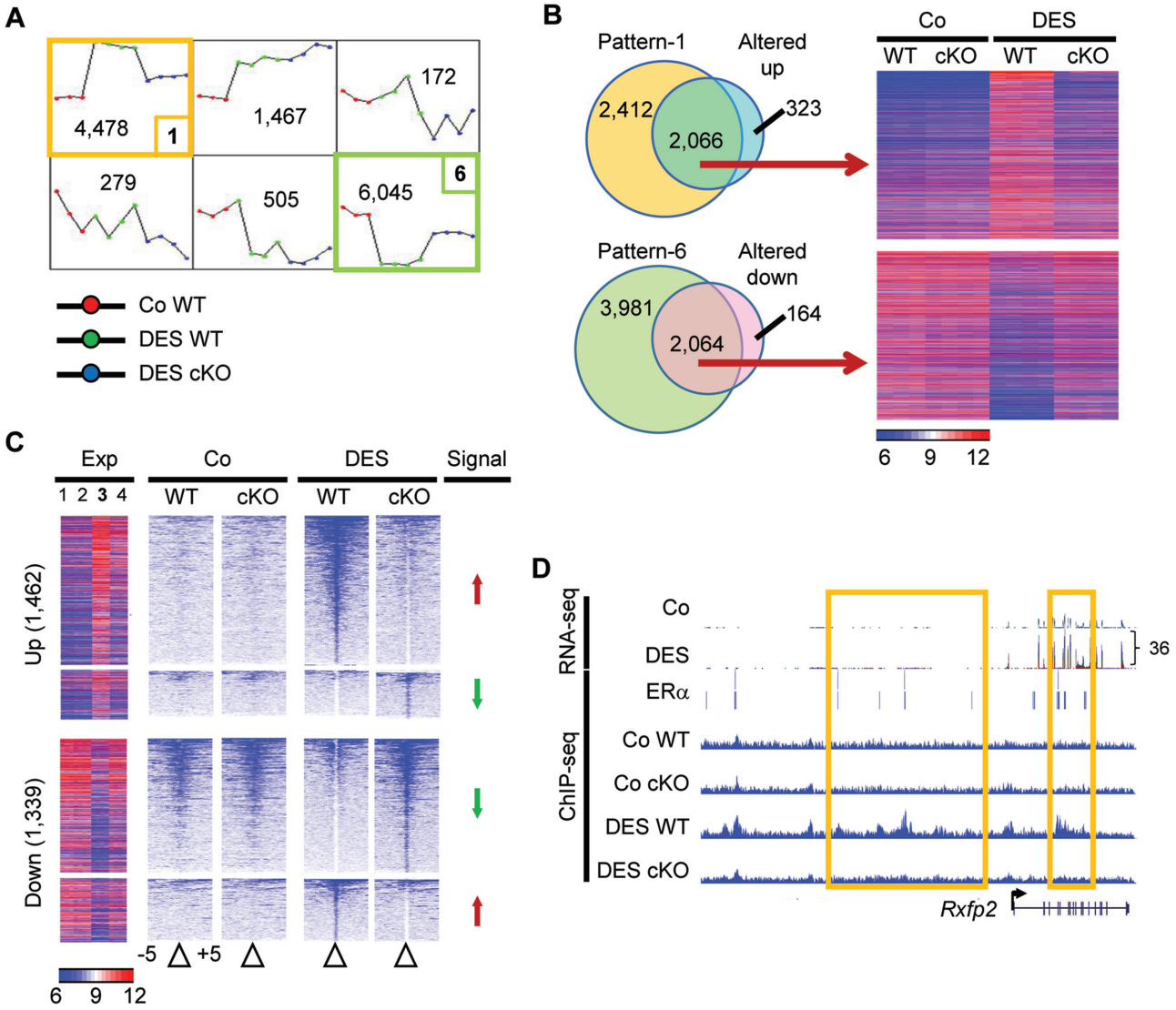

Figure 4. ERα is required for DES-induced gene expression and epigenetic modification. (**A**) Gene expression patterns (EPIG) of microarray data from Co-WT (red), DES-WT (green) and DES-Esr1 cKO (blue) samples ($n = 3$–4/group). Profiles of six gene expression patterns are shown; number of genes in each pattern is indicated in the box. The two gene expression patterns of interest are highlighted in gold (up-regulated genes) and green (down-regulated genes). (**B**) Venn diagram showing overlap between expression pattern-1 and up-regulated genes in microarray analysis comparison Co-WT versus DES-WT (2389). Venn diagram showing overlap between expression pattern-6 and down-regulated genes in microarray analysis comparison Co-WT versus DES-WT (2228). Heatmap representing the expression of up- and down-regulated genes that are protected by conditional uterine deletion of ERα. (**C**) Heat maps displaying differential H3K27ac signal at enhancers ±100 kb of 2801 genes protected from DES in Esr1 cKO (1422 up-regulated; 1,339 down-regulated). H3K27ac signal (±5 kb from center of the peak) shown in descending order based on the signal in the WT-DES sample and matched to gene expression changes between Co versus DES-exposed WT versus Esr1 cKO samples. Open triangle indicates center of peak. Top two panels, up-regulated genes; bottom two panels, down-regulated genes. The change in H3K27ac signal relative to gene expression is shown on the right; increased H3K27ac signal in WT DES compared to WT Co (red arrows) and decreased H3K27ac signal in WT DES compared to WT Co (green arrows). Expression (Exp): 1, Co-WT; 2, Co-Esr1 cKO; 3, DES-WT; 4, DES-Esr1 cKO. (**D**) Genome browser view of RNA-seq paired with ChIP-seq signal for H3K27ac and ChIP-seq tracks for ERα binding sites (43) from ovariectomized adult mice (top track, vehicle; bottom track, E2-1hr) at *Spsb1* locus. Gold boxes highlight regions that display a high density of ERα binding sites and differential H3K27ac enrichment following DES exposure that is not observed in the DES-Esr1 cKO sample.

deletions would also include those affected solely by the Foxa2 or Foxo1 deletion and not affected by DES exposure, indicating that Foxa2 and Foxo1 had a low impact on gene expression in this model system. To further examine the potential protection of DES induced gene changes by Foxa2 or Foxo1, we performed gene expression pattern analysis using EPIG on each of the new data sets compared with the previous microarray data set obtained from Esr1 cKO experiment (Co-WT and DES-WT). Despite the difference in background strains of these mice, 76% of probes from Foxa2 WT DES (9373 out of 12 377) and 72% of probes from Foxo1 WT DES (9458 out of 13 030) had a similar expression pattern to that in the Esr1 WT DES. For Foxa2, pattern 3 (172 genes), showed potential protection by Foxa2 deletion (Supplemental Figure S2B) and for Foxo1, patterns 6 and 7 (99 genes combined), showed

potential protection by Foxo1 deletion (Supplemental Figure S2C). We filtered these two patterns by genes that were significantly altered between Co-WT and DES-WT as described above. In contrast to the large overlap observed between DES-Esr1 cKO and genes significantly changed by DES treatment, only 82 out of 172 genes were significantly altered by DES and protected by uterine Foxa2 deletion and even fewer (29/99) were protected by uterine Foxo1 deletion (Supplemental Figure S2D). Gene expression patterns revealed only small changes in gene expression in the Foxa2 cKO and no distinct patterns in the Foxo1 cKO (Supplemental Figure S2D). Overall, these differences in gene expression were far less than the 4,073 protected by Esr1 cKO. Together, these data suggest that FOXA2 and FOXO1, despite their increased gene expression levels and enriched binding motifs in differential enhancer regions, do not contribute substantially to the overall impact of DES on uterine gene expression.

ERα is required for DES-mediated epigenetic modifications

The significant overlap between differentially bound H3K27ac enhancers in PND5 uteri and ERα binding sites observed in adult uteri suggested that acetylation of H3K27 at nucleosomes near ERα DNA elements (EREs) was a major mechanism by which DES exerts its effect on gene transcription. To test this idea, we utilized the Esr1 cKO mouse model and performed H3K27ac ChIP-seq on PND5 Co and DES-exposed WT and Esr1 cKO uteri. We first determined the differential H3K27ac enhancer peaks between Co-WT and DES-WT as described for Figure 3 and then determined how many of the 4130 Esr1 cKO protected genes had one or more of the H3K27ac differential peaks (Figure 4C). A comparison between the DES-WT versus DES-Esr1 cKO resulted in 12 817 differential H3K27ac peaks associated with 2964 of the 4130 protected genes (71.8%); 1462 and 1339 were up- and down- regulated, respectively. Similar to the ChIP-seq and gene expression-paired data described above, H3K27ac enriched genes were separated into up- or down-regulated groups and then ranked in descending order based on the highest number of reads for the H3K27ac peaks associated with each gene (Figure 4C). As expected, there was a robust increase in H3K27ac signal at most enhancers of genes up-regulated following DES treatment in the WT group (Figure 4C), similar to that observed in CD-1 mice (Figure 3A and E). Increased association of H3K27ac at up-regulated genes strongly correlated with higher gene expression, whereas low H3K27ac occupancy generally correlated with lower gene expression. Conditional deletion of uterine ERα abrogated DES induced effects as indicated by decreased H3K27ac association with these enhancer regions and the corresponding decrease in characteristic DES-induced changes in gene expression (Figure 4C).

Representative ChIP-seq profiles of H3K27ac and ERα-binding sites together with the associated gene expression of select upregulated genes are shown (Figure 4D and Supplemental Figure S3). For example, the *Rxfp2* gene, which was up-regulated following neonatal DES treatment, also displayed increased H3K27ac signal at an adjacent super-enhancer that overlapped with several ERα binding sites (Figure 4D). The DES-enriched H3K27ac signal was not observed in the DES-Esr1 cKO mice, demonstrating that ERα is necessary for the DES-induced gain of H3K27ac signal in this region. Another up-regulated gene, *Ltf*, showed a similar pattern with increased H3K27ac in the DES-WT and protection in the DES-Esr1 cKO (Supplemental Figure S3). Similar to CD-1 mice, the other minor pattern for up-regulated genes was decreased H3K27ac at a nearby enhancer, as shown for *Nxnl2* gene, where deletion of ERα reverts the DES induced loss of H3K27ac in this region (Supplemental Figure S3).

Similar associations between H3K27ac signal and altered gene expression were also observed for the down-regulated genes. The major pattern denoted the expected decrease in H3K27ac corresponding to the most down-regulated genes following DES exposure and gain of the signal to WT control levels in the DES-Esr1 cKO (Figure 4C, Lower panel). For example, *Col26a1* and *Hand2* were down-regulated and had decreased H3K27ac signal at nearby enhancers following DES treatment; the loss of H3K27ac was reversed in the absence of ERα (Supplemental Figure S3). In contrast, there was an increase in H3K27ac signal at enhancers near some of the down-regulated genes, suggesting active gene repression upon exposure to DES. Taken together, these data show that differential H3K27ac signal at enhancer regions near differentially expressed genes is a major mechanism by which DES exerts its effects on transcription and that deletion of ERα ablates this effect in the neonatal mouse uterus.

DES driven epigenetic modifications result in aberrant expression of the Padi gene family

To validate the global DES-induced epigenomic findings described above, we took a gene-specific approach to examine epigenomic modifications that might be involved in the altered gene expression. Several members of the peptidyl arginine deiminase *(Padi)* family, a class of genes not normally expressed in the neonatal uterus, were among those most highly up-regulated by neonatal DES treatment. The *Padi* genes include *Padi1*, *Padi2*, *Padi3*, *Padi4* and *Padi6*, all in a single locus on chromosome 4. Deimination of arginine residues by PADI enzymes results in their conversion to citrulline; this modification impacts the function of numerous proteins including histones (46–48). We first confirmed that the *Padi* family gene response to DES treatment was dependent on ERα. *Padi1, Padi2, Padi3, and Padi4* were all up-regulated by DES in our microarray dataset and conditional deletion of ERα abrogated this effect; this finding was confirmed by real time RT-PCR (Figure 5A). *Padi6* mRNA expression was very low in WT control mice and was unchanged by DES treatment. Consistent with the observed *Padi* gene upregulation, there was a dramatic increase in citrullinated proteins in uterine lysates following DES treatment (Figure 5B).

Using our H3K27ac ChIP-seq dataset, we identified a single differential H3K27ac enriched putative super-enhancer region upstream of the *Padi1* gene, whereas no differential H3K27ac peaks downstream of the TSS were

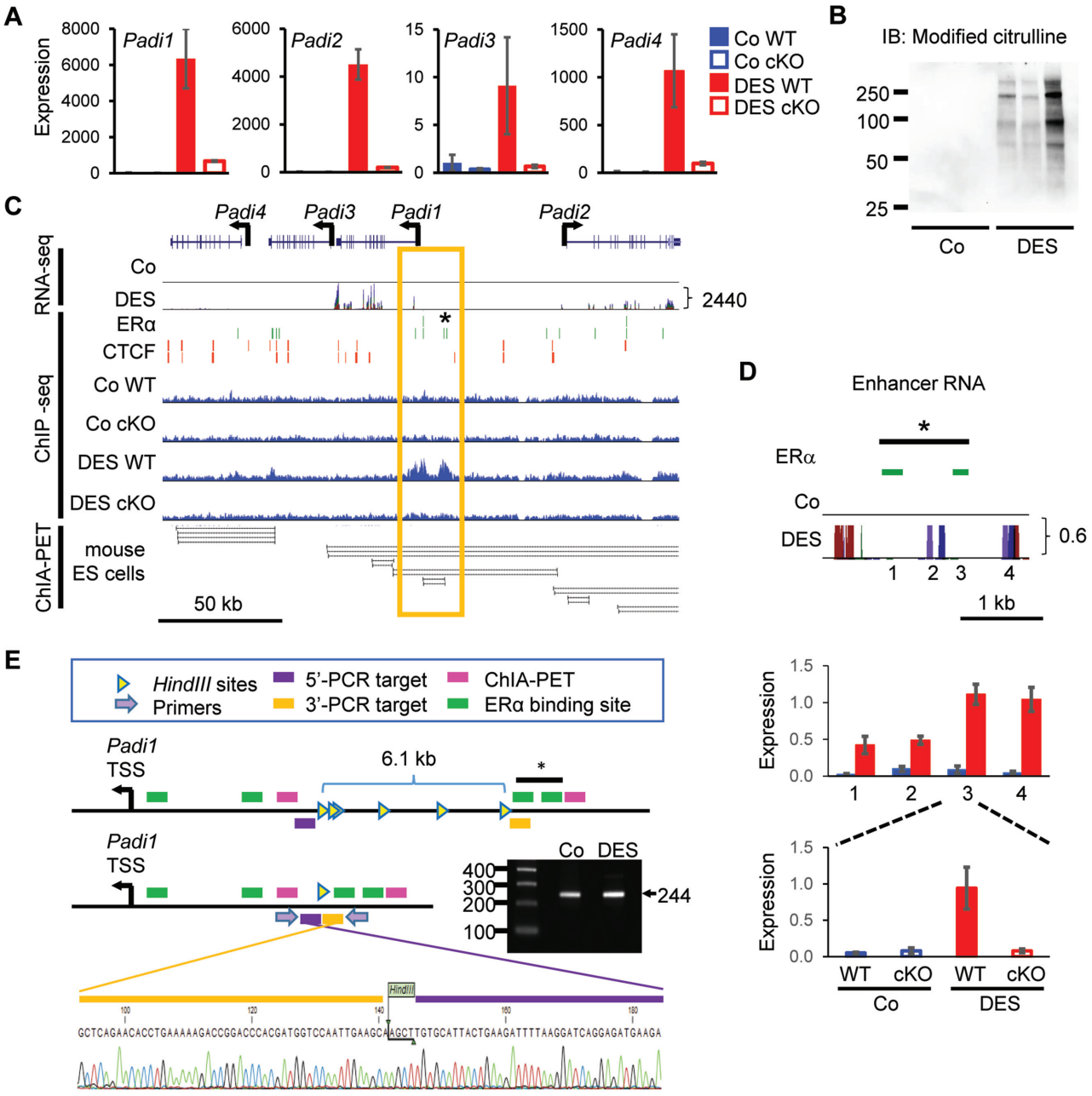

Figure 5. Altered Padi family gene expression depends on chromatin looping and ERα-mediated H3K27ac association. (**A**) Real time RT-PCR analysis of *Padi1-4* in Co and DES-exposed WT and Esr1 cKO uterine samples collected on PND5 ($n = 4$–6/group). Bar graphs show mean ± S.E.M. (**B**) Immunoblots of modified citrulline in 20 μg total protein lysate from uteri of Co and DES-exposed mice (n = 3/group). Molecular weight (kDa) indicated. (**C**) Browser tracks of RNA-seq, ChIP-seq (H3K27ac, ERα, and CTCF) and ChIA-PET at the *Padi* locus. ERα ChIP-seq tracks (43) from ovariectomized adult mice (top track, vehicle; bottom track, E2-1hr) shown in green. CTCF ChIP-seq tracks (49) from mouse liver (upper track) and ES cells (lower track) shown in orange. ChIA-PET tracks (51) are from mouse ES cells; dashed lines represent chromatin interactions. Gold box outlines a differentially H3K27ac associated region following DES exposure and protection from H3K27ac acquisition in the DES-Esr1 cKO. (**D**) Enhancer RNA (eRNA). Upper panel, RNA-seq tracks for Co and DES samples near the two ERα binding sites (green bars) denoted by the asterisk on panel C. Four locations near these two ERα binding sites (1–4) were selected to confirm the presence of eRNA by real time RT-PCR. Middle panel, graph of eRNA expression at locations 1–4 in Co and DES. Lower panel, graph of eRNA expression at location 3 in WT and Esr1 cKO mice, as indicated. Graphs show mean ± S.E.M. ($n =$ 3-4/group). (**E**) 3C-PCR at the *Padi1* enhancer/TSS loop. Schematic diagram of the *Padi* locus with regions of interest indicated. Asterisk indicates the two ERα binding sites marked in panels C and D. Schematic diagram of the *Padi* locus following *HindIII* excision and ligation of bound fragments. Gel electrophoresis of 3C-PCR products from uteri of Co and DES-exposed mice. Sequence chromatogram of excised band with regions of interest denoted. Results shown are representative of two independent biological replicates.

observed. Notably, the H3K27ac peaks in this region were observed in DES-WT samples but not in the DES-Esr1 cKO or either of the control groups (Figure 5C). These findings led us to hypothesize that the *Padi1-4* gene locus could be coordinately regulated by this super-enhancer. Coordinate gene regulation is accomplished in part by CTCF-mediated chromatin looping, which results in physical association of enhancer and promoter regions (49). In addition, CTCF is critical for ERα regulated chromatin interactions (50). To test whether DES-mediated gene expression at the *Padi* gene locus could involve specific chromatin interactions, we mined two published data sets, one identifying CTCF binding sites (49) and one identifying regions of chromatin interactions by chromatin interaction analysis by paired-end tag sequencing (ChIA-PET) (51). We then overlaid these data sets with published ERα ChIP-seq data (Hewitt *et al.*, 2012) and the H3K27ac ChIP-seq and RNA-seq from the current study (Figure 5C). Several ERα peaks overlapped with the H3K27ac peaks at the enhancer and TSS region of *Padi1* (Figure 5C). Furthermore, there was a single CTCF binding site near the *Padi1* enhancer region that also showed ChIA-PET interactions between the enhancer and *Padi1* TSS. There were several other CTCF binding sites in the *Padi1-4* locus as well as evidence of *Padi* gene interactions (*Padi1* to *Padi2* and *Padi3* to *Padi4,* Figure 5C). Collectively, these data support the possibility that DES-driven ERα-mediated changes in H3K27ac result in a chromatin state that allows coordinate regulation of the *Padi* gene locus through chromosome looping.

To confirm the activity of the enhancer upstream of Padi1, we tested for the presence of enhancer RNA (eRNA) in Co and DES-exposed uteri. eRNA transcript reads were detected by RNA-seq at the super-enhancer near two ERα binding sites in the DES-exposed group (Figure 5D). Analysis of eRNA expression by qRT-PCR at four regions close to the ERα binding sites demonstrated a significant increase in eRNA in DES-exposed uteri compared to controls (Figure 5D). Conditional deletion of ERα in the uterus abrogated eRNA expression, indicating that the eRNA transcription was ERα-dependent (Figure 5D). To determine whether looping of the *Padi1* promoter to the upstream enhancer occurred in uterine tissue, we performed chromatin conformation capture (3C) PCR (25). The previously reported ChIA-PET interactions (51) were used as the contact regions; a diagram of the experimental design is shown (Figure 5E). There were similar levels of PCR product in both Co and DES-exposed uterine samples, and sequencing of the amplicons confirmed the expected ligation product from loop formation (Figure 5E). To determine if the presence of ERα was required for loop formation, we also performed 3C real time PCR on Co WT, Co Esr1 cKO, DES WT and DES Esr1 cKO uterine samples. This loop was present in all four groups at almost identical levels (Ct values: Co WT, 20.5; Co Esr1 cKO, 20.8; DES WT, 21.0; DES Esr1 cKO, 20.7). These findings indicate that chromatin looping at this locus occurs *in vivo* in the developing uterus and that although the interaction is not dependent on ERα or DES exposure, H3K27ac enriched chromatin state and the resulting gene expression at this locus is DES and ERα-dependent.

DISCUSSION

Changes in chromatin architecture at gene regulatory regions upon exposure to compounds that mimic estrogen signaling have not been characterized using *in vivo* developmental model systems. This study reveals several key features of gene regulatory regions in the uteri of neonatal mice exposed to DES. First, genes whose expression changes upon DES treatment have a marked increase in H3K27ac signal at their promoters and enhancers, particularly if they are up-regulated. These sites represent new genomic loci that gain H3K27ac and not regions that are enriched with H3K27me3 and transition to H3K27ac. The vast majority of these changes depend on the presence of ERα, but not on the pioneer transcription factors, FOXO1 or FOXA2. However, it is possible that functional redundancy between these or other pioneer factors such as GATA3 explains the overall lack of gene expression changes in the single cKO models. Second, a small subset of genes with H3K27ac enriched enhancer signal are down-regulated, suggesting that enhancers are also involved in active repression. Third, active enhancer regions have a high binding density of ERα. Fourth, gene regulatory regions highly enriched with H3K27ac nucleosomes together with a high ERα and MED1 binding density have characteristic features of super-enhancers. Finally, coordinate gene regulation by chromosome looping is one mechanism by which DES dramatically impacts gene expression.

Histone H3K4me3 and H3K27me3 marks at promoter regions are usually associated with active transcription or transcriptional repression, respectively (52–55). However, here we found that these modifications do not account for DES mediated changes in gene expression. Perhaps this is not surprising as more recent genome wide studies show minimal changes in transcription upon removal of either H3K4me3 or H3K27me3, particularly under conditions where gene expression is at a steady state (56,57). EZH2 is the primary histone methyltransferase responsible for methylating histone H3K27 and a component of the polycomb repressive complex 2. Other components of this complex (JARID2, SUZ12, EED and RBAP46/48) are unchanged by DES exposure, but EZH2 is reduced ∼50% at the protein level [data from this paper and (5)]. Despite this reduction in EZH2, H3K27me3 is not different on a global scale by immunoblot (5) or at the TSS of altered genes during the time of exposure. Taken together, these findings indicate that a threshold level of EZH2 is sufficient to maintain global H3K27me3 marks as well as DES-induced, targeted H3K27me3 modifications.

Although H3K27ac associated enhancers are normally associated with active transcription, enhancer mediated gene repression, as shown here, has also been shown in other developmental model systems. For example, during dorsal-ventral (DV) axis formation in the *Drosophila* embryo, 'poised' enhancers that have relatively low levels of H3K27ac are observed when the nucleosome-free enhancer is targeted by a tissue specific repressor (58). A similar observation was made in *Drosophila* cell lines, where enhancer repression following hormone treatment causes recruitment of tissue specific repressors at ecdysone receptor-induced enhancers (59). In mouse ES cells, transcription at intra-

genic enhancers represses host gene expression (60). Together, these findings indicate that enhancer mediated repression is a conserved mechanism of gene regulation during development.

The regions we identified as super-enhancers based on their high enrichment of H3K27ac signal also have high binding density of ERα. These data suggest an important role for H3K27ac enriched super-enhancer regions in the DES exposure mouse model and that one of the major mechanisms by which DES impacts gene expression *in vivo* is by establishing highly accessible H3K27ac nucleosomes at ERα-bound super-enhancers. These findings are in agreement with studies demonstrating that H3K27ac enriched super-enhancers confer to cells and tissues the ability to activate and enhance transcription by increasing transcription factor density (in this case ERα) at specific loci to boost chromatin interactions that result in large changes in gene expression (11,24,33,61,62). Even more interestingly, this study unequivocally provides clear evidence that super-enhancer regions are highly sensitive to hormonal perturbation, which can ultimately lead to large changes in gene expression *in vivo* in the neonatal mouse uterus. Such changes in gene expression may drive key signaling pathways that explain the adverse effects of DES on the physiology and function of the reproductive tract *in vivo* (1,5,24,33,63).

Super-enhancers and associated transcription factors tend to control the expression of genes or families of genes that possess unique functions and play prominent roles in cell identity during development and tumorigenesis (33,64,65). One of the super-enhancers mis-regulated by DES treatment was in the genomic locus encoding the *Padi* gene family. The PAD (human) or PADI (mouse) enzymes convert arginine and methylarginine residues to citrulline through a hydrolytic process termed citrullination or deimination (66). Histones are PADI substrates, suggesting that mis-regulation of the *Padi* genes could have a major impact on chromatin architecture and ERα-mediated gene transcription. Indeed, PAD-mediated citrullination of histone H3 results in changes in gene expression of over 200 ERα target genes in MCF-7 breast cancer cell lines (67). Furthermore, histone H1 citrullination regulates mouse cell pluripotency, indicating a role for this modification in development (46). Because histone H1 citrullination leads to global chromatin decondensation, *Padi* upregulation could result in massive changes in gene transcription. The histone acetyltransferase primarily responsible for acetylating histone H3K27, p300, is also a substrate for PADI-mediated citrullination (68). Citrullination of p300 increases its binding to GRIP1 and this interaction is involved in estrogen-mediated signaling. The impact of increased protein citrullination, including that of histones, will be an exciting path for future research on mechanisms of DES action.

We propose a model (Figure 6) in which DES binds ERα at EREs of enhancers looped to the promoter regions of nearby estrogen target genes. This association results in differential H3K27ac modifications that are accentuated and prolonged because of the concomitant dramatic decrease in HDAC protein levels (5,69). Some of the largest changes in gene expression are associated with the presence of a super-enhancer where H3K27ac is accumulated in great excess. ERα is necessary for these events as shown by the conditional ERα deletion model where differential H3K27ac and altered gene expression is no longer observed. These changes in the epigenome likely contribute to the permanent alterations in gene expression observed in aged DES-exposed mice, and could also represent mechanisms by which other endocrine disrupting chemicals have long-term effects on development and adult physiology. Examining these and other epigenetic marks in adults using this model system will allow us to delineate the mechanisms by which permanent gene expression differences persist long after the exposure has ended and contribute to adult reproductive dysfunction and cancer.

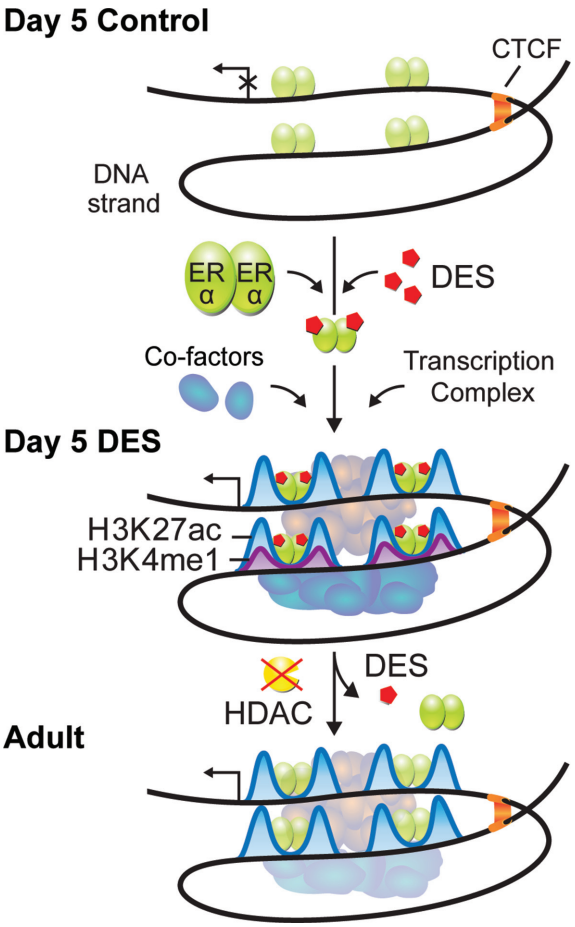

Figure 6. Working model of the toxicoepigenetics of neonatal DES exposure in mouse uteri. DES-induced changes in gene expression result from ERα-mediated H3K27ac association at topologically associating chromatin domains at the TSS and active enhancer regions (H3K4me1 and H3K27ac) of estrogen target genes. Pioneer transcription factors and/or other co-factors likely promote ERα actions. We propose that a decrease in HDAC protein expression following neonatal DES exposure (5) inhibits histone deacetylation, leading to hyperacetylation of H3K27ac (and possibly other histone lysine residues) at these regions and allowing transcription to persist even in the absence of estrogen.

DATA AVAILABILITY

Data analysis was performed on previousy published datasets as described in the Materials and Methods Section (43,49,51). Details of the software used in the current study can be found in Supplemental Table S1.

The raw and processed RNA-seq, microarray, and ChIP-seq datasets reported in this study were submitted to the NCBI Gene Expression Omnibus (www.ncbi.nlm.nih.gov/geo) with accession number GSE104402.

SUPPLEMENTARY DATA

Supplementary Data are available at NAR Online.

ACKNOWLEDGEMENTS

We thank Paul Wade, Christopher Lavender and Yin Li for critical review of this manuscript. We thank Kevin Gerrish for assistance with microarray and Nikki Reeves and Greg Solomon for assistance with library preparation, RNA-seq and ChIP-seq. We thank Ken Korach for providing the Esr1 floxed mice and Franco DeMayo for providing the Pgr-cre mice.

FUNDING

Intramural Research Program of the National Institutes of Health, National Institutes of Environmental Health Sciences [1ZIAES102405 to C.J.W., 1ZIAES071006 to T.A.]. Funding for open access charge: National Institutes of Health, National Institutes of Environmental Health Sciences.
Conflict of interest statement. None declared.

REFERENCES

1. Ho,S.-M., Cheong,A., Adgent,M.A., Veevers,J., Suen,A.A., Tam,N.N.C., Leung,Y.-K., Jefferson,W.N. and Williams,C.J. (2017) Environmental factors, epigenetics, and developmental origin of reproductive disorders. *Reprod. Toxicol.*, **68**, 85–104.
2. Newbold,R.R., Jefferson,W.N., Grissom,S.F., Padilla-Banks,E., Snyder,R.J. and Lobenhofer,E.K. (2007) Developmental exposure to diethylstilbestrol alters uterine gene expression that may be associated with uterine neoplasia later in life. *Mol. Carcinog.*, **46**, 783–796.
3. Suen,A.A., Jefferson,W.N., Wood,C.E., Padilla-Banks,E., Bae-Jump,V.L. and Williams,C.J. (2016) SIX1 Oncoprotein as a biomarker in a model of hormonal carcinogenesis and in human endometrial cancer HHS public access. *Mol. Cancer Res.*, **14**, 849–858.
4. Yin,Y., Lin,C., Veith,G.M., Chen,H., Dhandha,M. and Ma,L. (2012) Neonatal diethylstilbestrol exposure alters the metabolic profile of uterine epithelial cells. *Dis. Model. Mech.*, **5**, 870–880.
5. Jefferson,W.N., Chevalier,D.M., Phelps,J.Y., Cantor,A.M., Padilla-Banks,E., Newbold,R.R., Archer,T.K., Kinyamu,H.K. and Williams,C.J. (2013) Persistently altered epigenetic marks in the mouse uterus after neonatal estrogen exposure. *Mol. Endocrinol.*, **27**, 1666–1677.
6. Sato,K., Fukata,H., Kogo,Y., Ohgane,J., Shiota,K. and Mori,C. (2009) Neonatal exposure to diethylstilbestrol alters expression of DNA methyltransferases and methylation of genomic DNA in the mouse uterus. *Endocr. J.*, **56**, 131–139.
7. Tang,W.-Y., Newbold,R., Mardilovich,K., Jefferson,W., Cheng,R.Y.S., Medvedovic,M. and Ho,S.-M. (2008) Persistent hypomethylation in the promoter of nucleosomal binding protein 1 (Nsbp1) correlates with overexpression of Nsbp1 in mouse uteri neonatally exposed to diethylstilbestrol or genistein. *Endocrinology*, **149**, 5922–5931.
8. Bromer,J.G., Wu,J., Zhou,Y. and Taylor,H.S. (2009) Hypermethylation of homeobox A10 by *in Utero* diethylstilbestrol Exposure: An epigenetic mechanism for altered developmental programming. *Endocrinology*, **150**, 3376–3382.
9. Li,S., Hansman,R., Newbold,R., Davis,B., McLachlan,J.A. and Barrett,J.C. (2003) Neonatal diethylstilbestrol exposure induces persistent elevation of c-fos expression and hypomethylation in its Exon-4 in mouse uterus. *Mol. Carcinog.*, **38**, 78–84.
10. Bredfeldt,T.G., Greathouse,K.L., Safe,S.H., Hung,M.-C., Bedford,M.T. and Walker,C.L. (2010) Xenoestrogen-Induced regulation of EZH2 and histone methylation via estrogen receptor signaling to PI3K/AKT. *Mol. Endocrinol.*, **24**, 993–1006.
11. Liu,Z., Merkurjev,D., Yang,F., Li,W., Oh,S., Friedman,M.J., Song,X., Zhang,F., Ma,Q., Ohgi,K. *et al.* (2014) Enhancer activation requires Trans-Recruitment of a mega transcription factor complex. *Cell*, **159**, 358–373.
12. Carroll,J.S., Liu,X.S., Brodsky,A.S., Li,W., Meyer,C.A., Szary,A.J., Eeckhoute,J., Shao,W., Hestermann,E. V, Geistlinger,T.R. *et al.* (2005) Chromosome-Wide mapping of estrogen receptor binding reveals Long-Range regulation requiring the forkhead protein FoxA1. *Cell*, **122**, 33–43.
13. Ota,T., Suzuki,Y., Nishikawa,T., Otsuki,T., Sugiyama,T. and Pritchard,J.K. (2011) A User's guide to the encyclopedia of DNA elements (ENCODE). *PLoS Biol.*, **9**, e1001046.
14. Lupien,M., Eeckhoute,J., Meyer,C.A., Krum,S.A., Rhodes,D.R., Liu,X.S. and Brown,M. (2009) Coactivator function defines the active estrogen receptor alpha cistrome. *Mol. Cell. Biol.*, **29**, 3413–3423.
15. Jefferson,W.N., Padilla-Banks,E., Phelps,J.Y., Gerrish,K.E. and Williams,C.J. (2011) Permanent oviduct posteriorization after neonatal exposure to the phytoestrogen genistein. *Environ. Health Perspect.*, **119**, 1575–1582.
16. Chou,J.W., Zhou,T., Kaufmann,W.K., Paules,R.S. and Bushel,P.R. (2007) Extracting gene expression patterns and identifying co-expressed genes from microarray data reveals biologically responsive processes. *BMC Bioinformatics*, **8**, 427.
17. Trapnell,C., Pachter,L. and Salzberg,S.L. (2009) TopHat: discovering splice junctions with RNA-Seq. *Bioinformatics*, **25**, 1105–1111.
18. Trapnell,C., Williams,B., Pertea,G., Mortazavi,A., Kwan,G., van Baren,M.J., Salzberg,S.L., Wold,B.J. and Pachter,L. (2010) Transcript assembly and quantification by RNA-Seq reveals unannotated transcripts and isoform switching during cell differentiation. *Nat. Biotechnol.*, **28**, 511–515.
19. Langmead,B., Trapnell,C., Pop,M. and Salzberg,S.L. (2009) Ultrafast and memory-efficient alignment of short DNA sequences to the human genome. *Genome Biol.*, **10**, R25.
20. Zang,C., Schones,D.E., Zeng,C., Cui,K., Zhao,K. and Peng,W. (2009) A clustering approach for identification of enriched domains from histone modification ChIP-Seq data. *Bioinformatics*, **25**, 1952–1958.
21. Lienhard,M., Grimm,C., Morkel,M., Herwig,R. and Chavez,L. (2014) MEDIPS: Genome-wide differential coverage analysis of sequencing data derived from DNA enrichment experiments. *Bioinformatics*, **30**, 284–286.
22. Heinz,S., Benner,C., Spann,N., Bertolino,E., Lin,Y.C., Laslo,P., Cheng,J.X., Murre,C., Singh,H. and Glass,C.K. (2010) Simple combinations of lineage-determining transcription factors prime cis-regulatory elements required for macrophage and B cell identities. *Mol. Cell*, **28**, 576–589.
23. Huang,W., Loganantharaj,R., Schroeder,B., Fargo,D. and Li,L. (2013) PAVIS: a tool for peak annotation and visualization. *Bioinformatics*, **29**, 3097–3099.
24. Whyte,W.A., Orlando,D.A., Hnisz,D., Abraham,B.J., Lin,C.Y., Kagey,M.H., Rahl,P.B., Lee,T.I. and Young,R.A. (2013) Master transcription factors and mediator establish Super-Enhancers at key cell identity genes. *Cell*, **153**, 307–319.
25. Hagege,H., Klous,P., Braem,C., Splinter,E., Dekker,J., Cathala,G., De Laat,W. and Forne,T. (2007) Quantitative analysis of chromosome conformation capture assays (3c-qpcr). *Nat. Protoc.*, **2**, 1722–1733.
26. Huang,W.-W., Yin,Y., Bi,Q., Chiang,T.-C., Garner,N., Vuoristo,J., McLachlan,J.A. and Ma,L. (2005) Developmental diethylstilbestrol exposure alters genetic pathways of uterine cytodifferentiation. *Mol. Endocrinol.*, **19**, 669–682.
27. Creyghton,M.P., Cheng,A.W., Welstead,G.G., Kooistra,T., Carey,B.W., Steine,E.J., Hanna,J., Lodato,M.A., Frampton,G.M., Sharp,P.A. *et al.* (2010) Histone H3K27ac separates active from poised enhancers and predicts developmental state. *Proc. Natl. Acad. Sci. U.S.A.*, **107**, 21931–21936.

28. Calo,E. and Wysocka,J. (2013) Modification of enhancer chromatin: what, how, and why? *Mol. Cell*, **49**, 825–837.
29. Ernst,J. and Kellis,M. (2010) Discovery and characterization of chromatin states for systematic annotation of the human genome. *Nat. Biotechnol.*, **28**, 817–825.
30. Heinz,S., Romanoski,C.E., Benner,C. and Glass,C.K. (2015) The selection and function of cell type-specific enhancers. *Nat. Rev. Mol. Cell Biol.*, **16**, 144–154.
31. de Santa,F., Barozzi,I., Mietton,F., Ghisletti,S., Polletti,S., Tusi,B.K., Muller,H., Ragoussis,J., Wei,C.L. and Natoli,G. (2010) A large fraction of extragenic RNA Pol II transcription sites overlap enhancers. *PLoS Biol.*, **8**, e1000384.
32. Yan,L., Guo,H., Hu,B., Li,R., Yong,J., Zhao,Y., Zhi,X., Fan,X., Guo,F., Wang,X. *et al.* (2015) Epigenomic landscape of human fetal brain, heart, and liver. *J. Biol. Chem.*, **291**, 4386–4398.
33. Hnisz,D., Abraham,B.J.J., Lee,T.I.I., Lau,A., Saint-André,V., Sigova,A.A.A., Hoke,H.A.A. and Young,R.A.A. (2013) Super-enhancers in the control of cell identity and disease. *Cell*, **155**, 934–947.
34. Parker,S.C.J., Stitzel,M.L., Taylor,D.L., Orozco,J.M., Erdos,M.R., Akiyama,J.A., van Bueren,K.L., Chines,P.S., Narisu,N., Black,B.L. *et al.* (2013) Chromatin stretch enhancer states drive cell-specific gene regulation and harbor human disease risk variants. *Proc. Natl. Acad. Sci.*, **110**, 17921–17926.
35. Siepel,A., Bejerano,G., Pedersen,J.S., Hinrichs,A.S., Hou,M., Rosenbloom,K., Clawson,H., Spieth,J., Hillier,L.D.W., Richards,S. *et al.* (2005) Evolutionarily conserved elements in vertebrate, insect, worm, and yeast genomes. *Genome Res.*, **15**, 1034–1050.
36. McAninch,D., Thomas,P., Chandonia,J., Brenner,S. and Schaar,B. (2014) Identification of highly conserved putative developmental enhancers bound by SOX3 in neural progenitors using ChIP-Seq. *PLoS One*, **9**, e113361.
37. Couse,J.F., Dixon,D., Yates,M., Moore,A.B., Ma,L., Maas,R. and Korach,K.S. (2001) Estrogen receptor-alpha knockout mice exhibit resistance to the developmental effects of neonatal diethylstilbestrol exposure on the female reproductive tract. *Dev. Biol.*, **238**, 224–238.
38. Droog,M., Kim,Y., Nevedomskaya,E., Severson,T., Flach,K.D., Opdam,M., Schuurman,K., Gradowska,P., Hauptmann,M., Dackus,G. *et al.* (2016) Comparative cistromics reveals genomic cross-talk between FOXA1 and ERα in tamoxifen-associated endometrial carcinomas. *Cancer Res.*, **76**, 3773–3784.
39. Hah,N., Murakami,S., Nagari,A., Danko,C.G. and Lee Kraus,W. (2013) Enhancer transcripts mark active estrogen receptor binding sites. *Genome Res.*, **23**, 1210–1223.
40. Arnal,J.-F., Lenfant,F., Metivier,R., Flouriot,G., Henrion,D., Adlanmerini,M., Fontaine,C., Gourdy,P., Chambon,P., Katzenellenbogen,B. *et al.* (2017) Membrane and nuclear estrogen receptor alpha Actions: From tissue specificity to medical implications. *Physiol. Rev.*, **97**, 1045–1087.
41. He,H., Sinha,I., Fan,R., Haldosen,L.-A., Yan,F., Zhao,C. and Dahlman-Wright,K. (2018) c-Jun/AP-1 overexpression reprograms ERα signaling related to tamoxifen response in ERα-positive breast cancer. *Oncogene*, doi:10.1038/s41388-018-0165-8.
42. Guertin,M.J., Zhang,X., Anguish,L., Kim,S., Varticovski,L., Lis,J.T., Hager,G.L. and Coonrod,S.A. (2014) Targeted H3R26 deimination specifically facilitates estrogen receptor binding by modifying nucleosome structure. *PLoS Genet.*, **10**, e1004613.
43. Hewitt,S.C., Li,L., Grimm,S.A., Chen,Y., Liu,L., Li,Y., Bushel,P.R., Fargo,D. and Korach,K.S. (2012) Research Resource: Whole-Genome estrogen receptor α binding in mouse uterine tissue revealed by ChIP-Seq. *Mol. Endocrinol.*, **26**, 887–898.
44. Koen Dreijerink,A.M., Groner,A.C., Vos,E.S., Rao,P.K., Long,H.W., Brown Correspondence,M., Dreijerink,K.M., Font-Tello,A., Gu,L., Chi,D. *et al.* (2017) Enhancer-Mediated oncogenic function of the menin tumor suppressor in breast cancer. *Cell Rep.*, **18**, 2359–2372.
45. Wang,S., Sun,H., Ma,J., Zang,C., Wang,C., Wang,J., Tang,Q., Meyer,C.A., Zhang,Y. and Liu,X.S. (2013) Target analysis by integration of transcriptome and ChIP-seq data with BETA. *Nat. Protoc.*, **8**, 2502–2515.
46. Christophorou,M.A., Castelo-Branco,G., Halley-Stott,R.P., Oliveira,C.S., Loos,R., Radzisheuskaya,A., Mowen,K.A., Bertone,P., Silva,J.C.R., Zernicka-Goetz,M. *et al.* (2014) Citrullination regulates pluripotency and histone H1 binding to chromatin. *Nature*, **507**, 104–108.
47. Clancy,K.W., Russell,A.M., Subramanian,V., Nguyen,H., Qian,Y., Campbell,R.M. and Thompson,P.R. (2017) Citrullination/Methylation crosstalk on histone H3 regulates ER-Target gene transcription. *ACS Chem. Biol.*, **12**, 1691–1702.
48. György,B., Tóth,E., Tarcsa,E., Falus,A. and Buzás,E.I. (2006) Citrullination: A posttranslational modification in health and disease. *Int. J. Biochem. Cell Biol.*, **38**, 1662–1677.
49. Faure,A.J., Schmidt,D., Watt,S., Schwalie,P.C., Wilson,M.D., Xu,H., Ramsay,R.G., Odom,D.T. and Flicek,P. (2012) Cohesin regulates tissue-specific expression by stabilizing highly occupied cis-regulatory modules. *Genome Res.*, **22**, 2163–2175.
50. Fiorito,E., Sharma,Y., Gilfillan,S., Wang,S., Singh,S.K., Satheesh,S.V., Katika,M.R., Urbanucci,A., Thiede,B., Mills,I.G. *et al.* (2016) CTCF modulates estrogen receptor function through specific chromatin and nuclear matrix interactions. *Nucleic Acids Res.*, **44**, 10588–10602.
51. Kieffer-Kwon,K.-R., Tang,Z., Mathe,E., Qian,J., Sung,M.-H., Li,G., Resch,W., Baek,S., Pruett,N., Grøntved,L. *et al.* (2013) Interactome maps of mouse gene regulatory domains reveal basic principles of transcriptional regulation. *Cell*, **155**, 1507–1520.
52. Kouzarides,T. (2007) Chromatin Modifications and Their Function. *Cell*, **128**, 693–705.
53. Cao,R., Wang,L., Wang,H., Xia,L., Erdjument-Bromage,H., Tempst,P., Jones,R.S. and Zhang,Y. (2002) Role of histone H3 lysine 27 methylation in polycomb-group silencing. *Science*, **298**, 1039–1043.
54. Bernstein,B.E., Kamal,M., Lindblad-Toh,K., Bekiranov,S., Bailey,D.K., Huebert,D.J., McMahon,S., Karlsson,E.K., Kulbokas,E.J. III, Gingeras,T.R. *et al.* (2005) Genomic maps and comparative analysis of histone modifications in human and mouse. *Cell*, **120**, 169–181.
55. Santos-Rosa,H., Schneider,R., Bannister,A.J., Sherriff,J., Bernstein,B.E., Emre,N.C.T., Schreiber,S.L., Mellor,J. and Kouzarides,T. (2002) Active genes are tri-methylated at K4 of histone H3. *Nature*, **419**, 407–411.
56. Clouaire,T., Webb,S., Skene,P., Illingworth,R., Kerr,A., Andrews,R., Lee,J.H., Skalnik,D. and Bird,A. (2012) Cfp1 integrates both CpG content and gene activity for accurate H3K4me3 deposition in embryonic stem cells. *Genes Dev.*, **26**, 1714–1728.
57. De Kumar,B., Parrish,M.E., Slaughter,B.D., Unruh,J.R., Gogol,M., Seidel,C., Paulson,A., Li,H., Gaudenz,K., Peak,A. *et al.* (2015) Analysis of dynamic changes in retinoid-induced transcription and epigenetic profiles of murine Hox clusters in ES cells. *Genome Res.*, **25**, 1229–1243.
58. Koenecke,N., Johnston,J., He,Q., Meier,S. and Zeitlinger,J. (2017) Drosophila poised enhancers are generated during tissue patterning with the help of repression. *Genome Res.*, **27**, 64–74.
59. Shlyueva,D., Stelzer,C., Gerlach,D., Yá Ñ Ez-Cuna,J.O., Rath,M., Bory,Q.M., Arnold,C.D. and Stark,A. (2014) Hormone-responsive enhancer-activity maps reveal predictive motifs, indirect repression, and targeting of closed chromatin. *Mol. Cell*, **54**, 180–192.
60. Cinghu,S., Yang,P., Kosak,J.P., Conway,A.E., Kumar,D., Oldfield,A.J., Adelman,K. and Jothi,R. (2017) Intragenic enhancers attenuate host gene expression. *Mol. Cell*, **68**, 104–117.
61. Bojcsuk,O., Nagy,G. and Balint,B.L. (2017) Inducible super-enhancers are organized based on canonical signal-specific transcription factor binding elements. *Nucleic Acids Res.*, **45**, 3693–3706.
62. Fullwood,M.J., Liu,M.H., Pan,Y.F., Liu,J., Xu,H., Mohamed,Y.B., Orlov,Y.L., Velkov,S., Ho,A., Mei,P.H. *et al.* (2009) An oestrogen-receptor-alpha-bound human chromatin interactome. *Nature*, **462**, 58–64.
63. Sengupta,S. and George,R.E. (2017) Super-Enhancer-Driven transcriptional dependencies in cancer transcriptional deregulation in cancer. *Trends Cancer*, **3**, 269–281.
64. Lovén,J., Hoke,H.A., Lin,C.Y., Lau,A., David,A., Vakoc,C.R., Bradner,J.E., Lee,T.I. and Richard,A. (2013) Selective inhibition of tumor oncogenes by disruption of super-enhancers. *Cell*, **153**, 320–334.
65. Hnisz,D., Schuijers,J., Lin,C.Y.Y., Weintraub,A.S.S., Abraham,B.J.J., Lee,T.I.I., Bradner,J.E.E. and Young,R.A.A. (2015) Convergence of developmental and oncogenic signaling pathways at transcriptional Super-Enhancers. *Mol. Cell*, **58**, 362–370.

66. Thompson,P.R. and Fast,W. (2006) Histone citrullination by protein arginine deiminase: is arginine methylation a green light or a roadblock? *ACS Chem. Biol.*, **1**, 433–441.
67. Zhang,X., Bolt,M., Guertin,M.J., Chen,W., Zhang,S., Cherrington,B.D., Slade,D.J., Dreyton,C.J., Subramanian,V., Bicker,K.L. *et al.* (2012) Peptidylarginine deiminase 2-catalyzed histone H3 arginine 26 citrullination facilitates estrogen receptor target gene activation. *Proc. Natl. Acad. Sci. U.S.A.*, **109**, 13331–13336.
68. Lee,Y.-H., Coonrod,S.A., Kraus,W.L., Jelinek,M.A. and Stallcup,M.R. (2005) Regulation of coactivator complex assembly and function by protein arginine methylation and demethylimination. *Proc. Natl. Acad. Sci. U.S.A.*, **102**, 3611–3616.
69. Carleton,J.B., Berrett,K.C. and Gertz,J. (2017) Multiplex enhancer interference reveals collaborative control of gene regulation by estrogen receptor α-bound enhancers. *Cell Syst.*, **5**, 333–344.